Advances in Geo-Energy Research

Vol. 17, No. 2, p. 107-120, 2025

Original article

Microscopic insights into CO_2-shale oil miscibility via interaction energy coupled with pore confinement: Implications for CO_2-enhanced oil recovery

Xinran Yu[1,2], Haixin Dong[2], Yuxing Li[1,2]*, Cuiwei Liu[1,2], Linyang Zhang[3], Zhangxing Chen[4,5]

[1]*Shandong Provincial Key Laboratory of Oil, Gas and New Energy Storage and Transportation Safety, China University of Petroleum (East China), Qingdao 266580, P. R. China*

[2]*College of Pipeline and Civil Engineering, China University of Petroleum (East China), Qingdao 266580, P. R. China*

[3]*Key Laboratory of Industrial Fluid Energy Conservation and Pollution Control of the Ministry of Education, Qingdao University of Technology, Qingdao 266520, P. R. China*

[4]*Chemical and Petroleum Engineering, University of Calgary, Calgary, Alberta T2N1N4, Canada*

[5]*Eastern Institute of Technology, Ningbo 315200, P. R. China*

Keywords:
Minimum miscible pressure
confinement effect
miscibility
interaction energy

Cited as:
Yu, X., Dong, H., Li, Y., Liu, C., Zhang, L., Chen, Z. Microscopic insights into CO_2-shale oil miscibility via interaction energy coupled with pore confinement: Implications for CO_2-enhanced oil recovery. Advances in Geo-Energy Research, 2025, 17(2): 107-120.
https://doi.org/10.46690/ager.2025.08.03

Abstract:
As CO_2 injection can enhance the efficiency of shale oil extraction and reduce CO_2 emissions, it has been utilized widely in the development of shale oil resources. Minimum miscible pressure is an important parameter describing the miscibility of CO_2 and shale oil, which is of great importance for determination of CO_2 injection strategy. However, due to the unclear phase boundary caused by the confinement effect in shale nanopores, it is difficult to determine the minimum miscible pressure of CO_2 and shale oil. In this study, a new minimum miscible pressure estimation method is constructed, that is suitable for nanopores based on the significant co-evolution of pore wall adsorption and confined-bulk phase interactions. This method can mitigate the limitations of traditional minimum miscible pressure calculation methods relying on fluid interfaces. Furthermore, the confinement effects on the miscibility process are analyzed using a theoretical method and molecular dynamics simulation on the microscopic scale. The results demonstrate that the minimum miscible pressure of CO_2 and shale oil initially decreases as the pore size decreases. When the pore size decreases to a certain extent, the minimum miscible pressure increases with the thickness of the adsorbent layer rising and the CO_2 diffusion coefficient decreasing. Temperature elevation raises the minimum miscible pressure as it intensifies molecular thermal motion, weakens fluid adsorption, and reduces interaction energy, which are not conducive to miscibility. This study can provide an essential basis for the optimization of CO_2 injection pressure in shale oil reservoir development.

1. Introduction

Due to the increasing global energy demand, public interest has grown in the development of unconventional energy resources, such as shale oil and shale gas, which can complement fossil fuels to some extent. Horizontal drilling and hydraulic fracturing have enabled hydrocarbon production from unconventional reservoirs (Hou et al., 2019; Hui et al., 2023; Li et al., 2023). However, the recovery factor is still low because of the micro- and ultra-microscale pore structures in shale reservoirs (Dong and Hoffman, 2013; Pi et al., 2023).

Yandy Scientific Press

*Corresponding author.
E-mail address: joyyu94@163.com (X. Yu); dong620xin@163.com (H. Dong); lyxupc@163.com (Y. Li); chuyunlcw@163.com (C. Liu); linyang1412@yeah.net (L. Zhang); zhachen@ucalgary.ca (Z. Chen).

Received June 28, 2025; revised July 19, 2025; accepted July 30, 2025; available online August 3, 2025.

Recently, CO_2 has often been injected into shale formations to extract more hydrocarbon, attributed to its special physical-chemical properties (Rogala et al., 2014; Edwards et al., 2015; Alafnan, 2022). CO_2 is usually in a supercritical state under typical reservoir conditions; its density is similar to that of liquids and its viscosity is close to that of gases (Yu et al., 2020). Therefore, CO_2 in this state has strong diffusivity and can enter pores larger than its molecular diameter. When it contacts with shale oil in nanopores, it can dissolve in the oil. As a result, the viscosity of shale oil will decrease and a certain amount of unmovable oil can become movable (Liu et al., 2015; Zhang et al., 2020b; Wan et al., 2024). Furthermore, the injected CO_2 can also be stored in shale formations. As such, CO_2-enhanced shale oil recovery (CO_2-ESOR) can not only improve the recovery efficiency but also reduce emissions of anthropogenic CO_2.

Currently, there are two common methods for CO_2-ESOR, including CO_2 miscible flooding and CO_2 immiscible flooding. These two are distinguished by the minimum miscibility pressure (MMP), which helps to determine whether injected gas and shale oil can achieve a miscible state at the reservoir temperature. When the displacement pressure reaches the MMP, the interface between CO_2 and shale oil disappears and the two phases become a homogeneous single phase in the system. Thus, both the interfacial tension (IFT) between the oil and CO_2 phases and the capillary force decrease to zero. As a result, the theoretical displacement efficiency is improved, which indicates a higher recovery of shale oil. When the displacement pressure is below the MMP, the interface between CO_2 and shale oil still exists. On the one hand, a portion of the injected CO_2 dissolves in shale oil; on the other hand, a fraction of light components in shale oil evaporates into CO_2. Thus, the oil volume expansion can be observed, and the oil viscosity and the IFT between CO_2 and shale oil decrease correspondingly (Yuan et al., 2023). Although the oil displacement efficiency shows an overall improvement, it is still much lower than that of CO_2 miscible flooding (Lashgari et al., 2019). Therefore, to determine the CO_2 injection strategy, it is of great significance to estimate the MMP in the CO_2-shale oil system.

Unlike in conventional reservoirs, large numbers of micro- and ultra-micropores exist in shale reservoirs (Li et al., 2016, 2018; Wu et al., 2016). The confinement of pore walls on fluid in shale reservoirs can lead to dramatic changes in the fluid properties, such as IFT and critical point, which makes the mixing process of CO_2 and shale oil within the nanopores different from that of their bulk phases (Dong et al., 2023). Huang carried out experiments on the mixture of CO_2 and shale oil within nanopores (Huang et al., 2020) and found that the MMP at the nanopore scale was larger than that at the micrometer scale. This is because the perturbation of phase interface within the nanopore is mainly dominated by the flow induced by the pressure gradient. The flow velocity decreases at the phase interface in nanopores, and the perturbation of phase interface becomes weaker. Therefore, the mass transfer between CO_2 and shale oil is limited. Additionally, the inhibition of miscibility can be observed as the pore size decreases from 5 to 2 nm, which is attributed to the adsorption layer of shale oil (Fang et al., 2019; Sun et al., 2023). In smaller pores, the amount of adsorbed shale oil increases, and the amount of free shale oil decreases correspondingly. Therefore, the miscibility of CO_2 and shale oil is weakened in pores smaller than 5 nm. However, the miscible state can still be easily achieved compared to the bulk phase. Different conclusions were obtained by other scholars, who reported that, based on the semi-analytical Equation of State (EOS), the miscibility of the CO_2 and shale oil system is enhanced as the pore size decreases (Zhang et al., 2018b). Moreover, the effect of nanopore size on MMP was analyzed using the modified Peng-Robinson EOS: The MMP increased rapidly with increasing pore size when the pore size was smaller than 10 nm, while this increasing trended tends to slow down when the pore size increased to a certain value (Bu et al., 2023). Therefore, the effects of confinement on the mass transfer between CO_2 and oil phases and the miscibility of CO_2 and oil in the confined pore are still unclear and need to be further investigated.

As reported in the literature, the MMP can be determined by various experimental techniques, such as slim-tube tests (Hawthorne et al., 2016; Dong et al., 2019; Abdurrahman et al., 2023), the rising bubble apparatus (Safaei et al., 2021), and the vanishing IFT (VIT) (Hawthorne et al., 2020; Lv et al., 2023). However, these experimental systems for MMP prediction are complex and time-consuming (Liu et al., 2025), and they cannot accurately determine the MMP in confined pores. Since the pore size in shale reservoirs ranges from 5 to 1,000 nm (Firouzi et al., 2014), some empirical models ranging from temperature-dependent to multifactor-dependent ones were developed for a convenient estimation of the MMP under the reservoir conditions (Hassan et al., 2019; Mohammadian et al., 2024). Zhang et al. (2018a) proposed a correlation that considers the effect of confined space. Moreover, theoretical models based on the EOS, such as Peng-Robinson EOS and cubic EOS coupling the effects of pore size distribution, capillary pressure, critical point shift, and confinement, were developed for the MMP calculation (Sun and Li, 2019). Among them, the modified method of characteristics developed by Teklu et al. (2014) was found to be promising for the MMP determination in confined pores. However, the volume translation model was not considered in the algorithm and this can lead to inaccurate phase density in the confined pore, further resulting in the incorrect determination of MMP for the CO_2 and shale oil in nanopores. Besides, the development of these empirical models is usually dependent on experimental data, and they cannot be applied under some complex scenarios.

Recently, molecular dynamics (MD) simulation has shown great benefits in describing gas-liquid-solid intermolecular interactions. This method can be used to investigate physical phenomena in shale reservoirs, such as adsorption, wetting and flow, from the microscopic perspective (Zhang et al., 2020a; Yu et al., 2021). Some researchers conducted MD simulations for the MMP calculation, providing supplementary results to experiments (Peng et al., 2018; Wang et al., 2018; Wu et al., 2024). Similar to experimental techniques, the VIT method is employed in these studies: The IFT is determined by MD simulations and plotted with different pressures, and the MMP

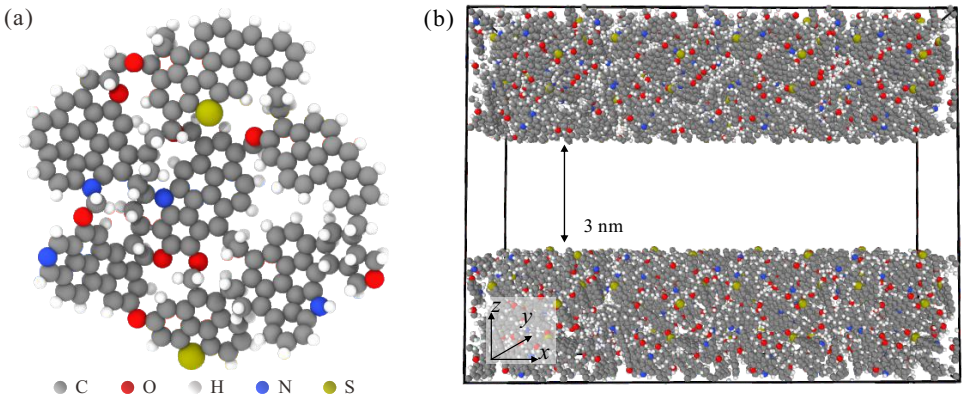

Fig. 1. (a) Snapshot of the kerogen type II-D unit mode and (b) kerogen slit pore with a pore size of 3 nm.

corresponds to the pressure when the IFT is zero. The MD simulations mentioned above investigate the miscibility in the bulk phase. As for nanopores, the interfacial thickness is determined on the basis of the Gibbs dividing surface to characterize the miscible process of CO_2 and *n*-decane (Fang et al., 2019). When the interfacial thickness is stable, the MMP can be achieved (Zhang et al., 2017). Furthermore, Sun et al. (2023) estimated the MMP by conducting CO_2 huff-n-puff MD simulation. They achieved the calculation of MMP on the basis of the plot displaying the relationship between recovery rate and fluid pressure. They found that the recovery rate increases with the pressure and tends to be stable when the pressure increases to a threshold value. The MMP corresponds to the intersection of the two fitting lines for the recovery factor below and after the sharp turning point. However, the Gibbs dividing surface (GDS)-based method for calculating interfacial thickness is limited by the difficulty of accurately determining the gas-liquid interface. Meanwhile, the method based on the recovery rate is constrained by the simplified assumptions of physical models. Thus, neither of these methods can be effectively applied to determine the MMP in nanopores with clear physical meanings.

In this study, to investigate the miscibility of CO_2 and shale oil in nanopores under the *in-situ* shale reservoir conditions, MD simulations are conducted using a Large-scale Atomic/Molecular Massively Parallel Simulator (Plimpton, 1995). Different from traditional methods that rely on bulk phases or simplified models, this study aims to reveal the influencing mechanism of the pore confinement effect on the thermodynamics and kinetics of miscibility at the molecular scale. By constructing an energy characterization system, a miscible pressure estimation method is established that is suitable for nanopores, with the energy difference (δE) of bulk phase and pore phase, so as to break through the bottleneck of the existing MMP determination method that relies on phase interfaces.

2. Methodology

2.1 Model construction

The scanning electron microscope can be used to characterize the pore structure, including pore size, pore geometry, and pore network. Slit-like and cylindrical pores can be found in shales (Bu et al., 2015). In our work, slit-like pores are investigated because of their high abundance in the shale reservoirs, and also because fluid distribution in this kind of pores is similar to the cylindrical pores with an equal size. The kerogen unit used in our simulation is type II-D kerogen, which is a typical organic matter in shale reservoirs, such as the Barnett Shale (Ungerer et al., 2015). The chemical formula of the unit model is $C_{175}H_{102}O_9N_4S_2$ developed by Ungerer et al. (2015), as displayed in Fig. 1(a). The elemental analysis and the functional group analysis results of this kerogen unit match well with the experimental results (Raza et al., 2022).

The pore model of shales built in our work is of a slit-like pore consisting of 32 kerogen unit models in each wall. The dimensions of each pore wall are 11.53, 2.88 and 2.88 nm along the *x*-, *y*- and *z*-axis, respectively. The pore size is defined as the distance between the inner surfaces of pore walls, and the three-dimensional periodical boundary condition is applied in all simulations. To build the kerogen pore wall, 32 kerogen unit models are placed in a simulation cell of 11.54 nm × 10 nm × 10 nm. The length of the simulation cell is kept constrained, and the width and height are flexible. A consistent valence force field is applied for the kerogen model (Collell et al., 2014; Liu et al., 2022), and the steps for pore wall construction can be found in this study (Yu et al., 2021). Finally, the kerogen porous model in Fig. 1(b) can be obtained with a density of 1.3 g/mL at 300 K and 0.1 MPa, which is consistent with literature data (Stankiewicz et al., 2015; Ungerer et al., 2015). This model consists of both the slit pore and porous media of kerogen, which can be used to investigate the mixing and adsorption process.

Different model configurations are built to investigate the MMP in the bulk phase and in the confined pore. Fig. 2 displays the CO_2 and shale oil system in the simulation cell with 11.54 nm × 2.88 nm × 8.77 nm. In all simulation cases, *n*-decane ($C_{10}H_{22}$) is used to characterize the crude oil in shale reservoirs. The number of *n*-decane is kept at 100 for kerogen slit pore with a pore size of 3 nm, while the number of CO_2 molecules is changed to maintain the system pressure. The numbers of CO_2 molecules in different cases are displayed in Table 1. The amounts of *n*-decane and CO_2 in the system we-

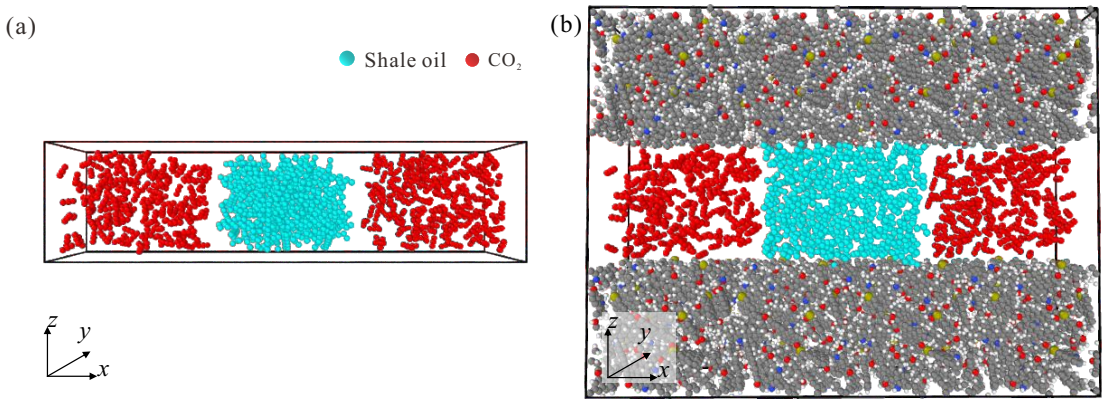

Fig. 2. Initial system of CO_2 and shale oil: (a) Bulk and (b) 3 nm organic slit pore.

Table 1. Number of CO_2 and *n*-decane molecules in simulation cases at 343 K.

Pore size (nm)	Injection pressure *p* (MPa)	Number	
		CO_2	*n*-decane
Bulk	5	86	100
	7	132	100
	9	190	100
	11	270	100
	13	368	100
3	5	86	100
	7	132	100
	9	190	100
	11	270	100
	13	368	100
5	5	142	165
	7	218	165
	9	318	165
	11	448	165
	13	612	165
10	5	284	330
	7	436	330
	9	634	330
	11	894	330
	13	1,224	330

re calculated based on the densities at corresponding temperatures and pressures in the National Institute of Standards and Technology Experimental Database.

The Lennard-Jones (L-J) potential function was used to describe the interaction force between atoms, which is given by (Plimpton, 1995):

$$\varphi_{ij} = 4\varepsilon_{ij}\left[\left(\frac{\sigma_{ij}}{r_{ij}}\right)^{12} - \left(\frac{\sigma_{ij}}{r_{ij}}\right)^{6}\right] \tag{1}$$

where r_{ij} represents the distance between atoms of type i and type j; ε_{ij} represents the potential well depth of the L-J potential, which characterizes the interaction strength between atoms; σ_{ij} represents the distance at which the interaction energy between two particles is the minimum.

The cross-interaction terms between different molecules are calculated using the Lorentz-Berthelot mixing rule, which is expressed by (Plimpton, 1995):

$$\sigma_{ij} = \frac{1}{2}(\sigma_{ii} + \sigma_{jj}) \tag{2}$$

$$\varepsilon_{ij} = \frac{1}{2}\sqrt{\varepsilon_{ii}\varepsilon_{jj}} \tag{3}$$

The long-range Coulomb force between atoms is expressed by (Plimpton, 1995):

$$U_{coul} = \frac{q_i q_j}{4\pi\varepsilon_0 r_{ij}} \tag{4}$$

where q_i and q_j represent the charges of atoms of type i and type j, respectively; ε_0 is the dielectric constant of vacuum.

The Transferable Potentials for Phase Equilibria (TraPPE) force field and TraPPE United Atom (TraPPE-UA) force field are applied to simulate CO_2 molecules and *n*-decane molecules, respectively. The thermodynamic and equilibrated vapor-liquid properties of CO_2 and *n*-decane can be reproduced by the TraPPE force field (Dinpajooh et al., 2015; Zhan et al., 2020). The Lennard-Jones parameters for these two kinds of molecules are shown in Table 2, and the bond and angle of CO_2 are kept rigid in the simulation (Tables 3 and 4).

2.2 Molecular simulation details

In order to investigate the confinement effect, the binary system of CO_2 and shale oil is placed in the kerogen slit pore with the pore size of 3, 5, and 10 nm. The mass transfer processes of CO_2 and shale oil in unconfined and confined spaces under different pressures (5, 7, 9, 11 and 13 MPa) are simulated to obtain the controlling effect of pressure on the process and to calculate the MMP of CO_2 and shale oil. The recovery mechanism of shale oil is investigated from a micro-

Table 2. L-J parameters employed for *n*-decane and CO_2 in the simulations.

Atom type	Mass (g/mol)	ε/K_B (K)	σ (nm)	q (e)
CH_3 (*n*-decane)	15.035	98.00	0.375	0
CH_2 (*n*-decane)	14.027	46.00	0.395	0
C (CO_2)	12.011	27.00	0.280	0.70
O (CO_2)	15.999	79.00	0.305	-0.35

Notes: K_B is Boltzmann constant.

Table 3. Bond parameters employed for *n*-decane and CO_2 in the simulations.

Bond type	k_r (K/nm^2)	σ (nm)
CH_3-CH_2	4,820,000	0.154
CH_2-CH_2	4,820,000	0.154
C−O	Rigid	0.116

Notes: K_r is the harmonic constants.

Table 4. Angle parameters employed for *n*-decane and CO_2 in the simulations.

Angle type	k_θ/K_B (K/rad^2)	θ (deg)
$CH_3-CH_2-CH_2$	62,500	114
$CH_2-CH_2-CH_2$	62,500	114
O−C−O	Rigid	180

Notes: k_θ is the harmonic constants; θ is the equilibrium angle.

scopic perspective.

All simulation calculations in this study are conducted in the NVT ensemble, with temperature controlled using a Nosé-Hoover thermostat, in order to simulate the mass transfer processes at 343 K and 363 K. Periodical boundary conditions are applied along all directions and the Verlet algorithm is used to solve Newton's equations of motion. As the L-J interaction ends at 1 nm, cases at all pressures are simulated for 5 ns with a timestep of 1 fs to obtain the system equilibrium and another 2 ns is run for data collection.

2.3 Relative concentration

The distribution of CO_2 and shale oil in the slit can be quantitatively compared and analyzed based on the relative concentrations perpendicular to the slit direction. The relative concentration is defined as the ratio of the concentration of a selected molecule in a certain area to the average concentration of the molecule in the system, which can be calculated by (Wu et al., 2024):

$$C_r = \frac{C_v}{C_t} \tag{5}$$

$$C_v = \frac{n_v}{V_v} \tag{6}$$

$$C_t = \frac{n_t}{V_t} \tag{7}$$

where C_r represents the relative concentration of a component perpendicular to the wall; C_v represents the concentration of a molecule in a small piece perpendicular to the wall, mol/L; C_t represents the average concentration of a component in the system, mol/L; n represents the amount of a component substance, mol; V is the volume of a component, L.

2.4 Diffusion coefficient

The rate of mixing between CO_2 and shale oil molecules can be described based on the diffusion coefficient. The self-diffusion coefficients D for shale oil and CO_2 are calculated based on the mean square displacement (MSD) using the Einstein relation (Allen and Tildesley, 2017):

$$D = \lim_{t\to\infty} \frac{1}{6t} \left\langle |r_i(t) - r_i(0)|^2 \right\rangle \tag{8}$$

The MSD reflects the average displacement of a molecule over a certain period of time, where $\left\langle |r_i(t) - r_i(0)|^2 \right\rangle$ represents the MSD of the molecule at time t relative to its initial position. In MD simulations, the coordinate information of shale oil and CO_2 molecules at each time step can be recorded in detail, and then their MSD in different time periods can be calculated. By substituting the calculated MSD data into Eq. (8), the self-diffusion coefficient D of shale oil and CO_2 can be determined, which can quantitatively describe the diffusion capacity and rate of shale oil and CO_2 molecules in the system, providing an important quantitative basis for further investigating the mixing process between CO_2 and shale oil molecules.

2.5 IFT

The MMP of the CO_2 and shale oil system in the bulk phase can be obtained by the VIT method, which is based on the characteristic that the IFT changes with pressure: When the system pressure reaches the MMP, the IFT between the two phases gradually decreases and approaches zero, and the two fluids reach a miscible state at this point (Peng et al., 2018). To accurately measure the IFT between CO_2 and shale oil in the bulk phase, an interface perpendicular to the x-axis is constructed using simulation methods. On the basis of the GDS theory (Fang et al., 2019; Lv et al., 2023), the concentration distribution curve of shale oil along the x-axis is fitted by the following formula to determine the two-phase interface of CO_2 and shale oil, as shown in Fig. 3:

$$\rho(x) = \frac{1}{2}\rho_0 \left[\mathrm{erf}\left(\frac{x-x_1}{\sigma\sqrt{2}}\right) - \mathrm{erf}\left(\frac{x-x_2}{\sigma\sqrt{2}}\right) \right] \tag{9}$$

where ρ_0 represents the bulk concentrations of shale oil under the temperature and pressure conditions of the system; x_1 and x_2 represent the position of the Gibbs dividing surface, and σ is the standard deviation of the distance.

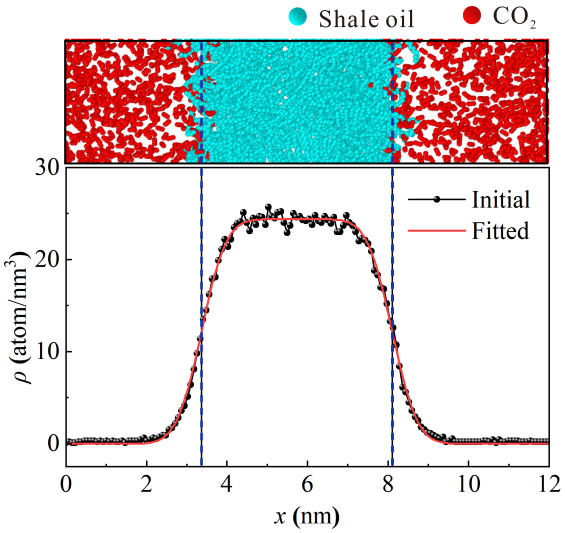

Fig. 3. Interface between CO_2 and shale oil divided based on the GDS theory.

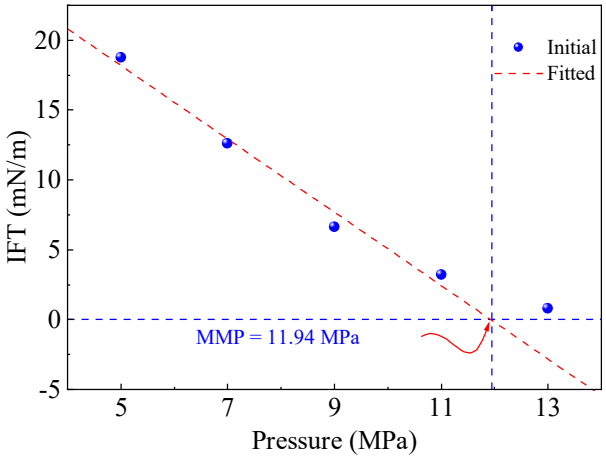

Fig. 4. Variation in IFT between CO_2 and shale oil in bulk phase with pressure at 343 K.

The IFT between CO_2 and shale oil is calculated on the basis of the pressure tensor (Fang et al., 2019):

$$\gamma = \frac{1}{2}\int_0^{l_x} [P_n(x) - P_t(x)]\,\mathrm{d}x = \frac{1}{2}\left(P_{xx} - \frac{P_{yy}+P_{zz}}{2}\right) l_x \quad (10)$$

where P_n and P_t represent normal pressure and tangential pressure, respectively; P_{II} $(I = x,\ y,\ z)$ represents pressure tensor; l_x represents the length of the shale oil in the x-axis direction, calculated by $x_2 - x_1$. The pore pressure is calculated using the symmetric stress tensor output by LAMMPS.

On the basis of the simulation results, the data are processed by linear regression, and the regression curve is shown in Fig. 4. By further extending the regression curve to intersect with the pressure axis, the miscibility pressure when the CO_2 and shale oil IFT is 0 can be obtained, which is the MMP.

2.6 Characterization of the confinement effect

The confinement effect in nanopores can lead to a strong adsorption of shale oil and CO_2 on the kerogen wall, as well as different mixing behavior between shale oil and CO_2 compared to the bulk phase (Sun et al., 2023). To quantify this difference, the effect of restriction on fluid distribution can be described by defining δE:

$$\delta E = E_s - E_b \quad (11)$$

where E_b is the interaction energy in the bulk phase; E_s is the interaction energy in the nanoslits.

The interaction energy of the bulk fluid (E_b) refers to the interaction energy between CO_2 and shale oil in the bulk, where the interaction energy between individual molecules can be calculated by Eq. (1). Therefore, E_b can be expressed by (Prasetyo et al., 2018):

$$E_b = \int \varphi_{ff}\rho_b(z)\mathrm{d}z \quad (12)$$

where ρ_b represents the molecular number density of CO_2 and shale oil in the bulk phase.

The interaction energy in the nanoslits (E_s) includes the fluid-fluid interaction energy φ_{ff} and the wall-fluid interaction energy φ_{sf}, due to the particularity of the wall, which can be described by (Prasetyo et al., 2018):

$$\varphi_{sf} = 2\pi\varepsilon\sigma^2\left[\frac{2}{5}\left(\frac{\sigma_{ij}}{r_{ij}}\right)^{10} - \left(\frac{\sigma_{ij}}{r_{ij}}\right)^{4}\right] \quad (13)$$

$$E_s = \int \left(\varphi_{sf} + \varphi_{ff}\right)\rho_s(z)\mathrm{d}z \quad (14)$$

where ρ_s represents the molecular number density of CO_2 and shale oil in the nanoslits.

Due to the limitation of pore geometry and potential energy, the spatial range that the fluid molecules can reach is limited. The maximum accessible volume of molecules in the pores V_Ω can be determined by:

$$V_\Omega = l_x l_y (z_1 - z_2) \quad (15)$$

where l_x denotes the length of the system along the x-axis; l_y denotes its length along the y-axis; z_1 and z_2 represent the demarcation boundary of the accessible volume of molecules in pores, which can be solved via (Prasetyo et al., 2018):

$$\int_z^\infty [-\varphi(z)]\,\mathrm{d}z = 0 \quad (16)$$

where $\varphi(z)$ is the potential energy between fluid molecules and the wall.

Thus, by substituting Eqs. (13) and (15) into Eq. (11), δE can be calculated by:

$$\delta E = \int_{V_\Omega} \left(\varphi_{sf} + \varphi_{ff}\right)\rho_s(z)\mathrm{d}z - \int_{V_b} \varphi_{ff}\rho_b(z)\mathrm{d}z \quad (17)$$

Since the number of molecules in the bulk phase and pores is the same, and the molecular number density satisfies the normalization constraint, Eq. (17) can be further simplified as:

$$\delta E = \int_{V_\Omega} \left\{\varphi_{sf}\rho_s(z) + \varphi_{ff}\left[\rho_s(z) - \rho_b(z)\right]\right\}\mathrm{d}z \quad (18)$$

The first term in Eq. (18) represents the adsorption energy of pore wall, which results from the interaction between wall and fluid. The second term characterizes the difference in the interaction energy between the confined and bulk fluid, which

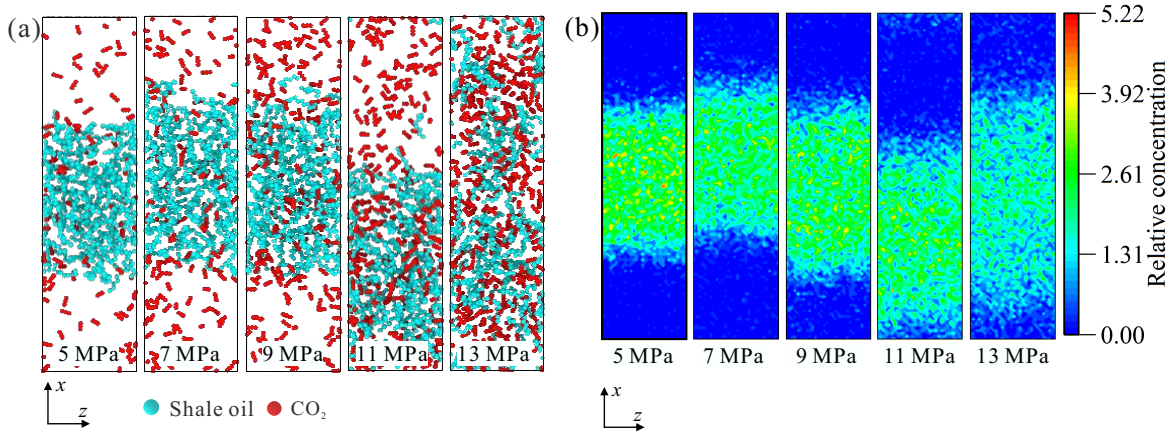

Fig. 5. (a) Simulation snapshots of CO_2 and shale oil and (b) cloud diagram of concentration distribution of shale oil in bulk phase at 343 K.

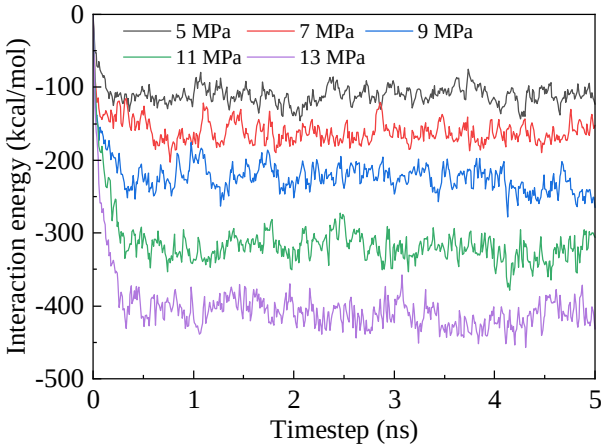

Fig. 6. Interaction energy between CO_2 and shale oil in bulk phase at 343 K.

is attributed to the energy perturbation caused by the change in molecular arrangement. When the system conditions change, the energy balance is broken by the energy difference between pore wall adsorption and pore-bulk phase interaction: The negative feedback of the adsorption energy difference decreases when the pressure increases; at the same time, the fluid density distribution tends to be uniform, and the positive feedback of the pore-bulk phase energy difference decreases, which synergistically weakens the phase transformation energy barrier. The thermal movement of fluid molecules makes it easier to break through the barrier, which promotes the transfer of CO_2 and shale oil from a non-miscible state to a miscible state.

3. Results and discussion

3.1 Miscible behavior in bulk phase

At 343 K, the IFT between CO_2 and shale oil in bulk phase decreased almost monotonically and linearly with increasing pressure, as shown in Fig. 4. By extrapolating the linear regression line of the IFT-pressure curve to zero, the CO_2-shale oil MMP of 11.94 MPa was obtained for the bulk phase, which is highly consistent with the value of 11.76 MPa measured by Shaver et al. (2001) at 344 K.

The snapshots of the simulation process presented in Fig. 5(a) clearly demonstrate the characteristics of phase evolution under pressure regulation: As the system pressure gradually increases, CO_2 molecules in the bulk phase continuously break through the phase interface, gradually permeating, dissolving, and diffusing into the oil phase. Meanwhile, this process continuously drives the gradual expansion of shale oil molecules, whose spatial arrangement gradually stretches out from the initial state of local aggregation, eventually forming a homogeneously distributed mixed system in the bulk phase. The characteristics of shale oil concentration distribution (Fig. 5(b)) further confirms this trend: At the low-pressure stage, shale oil concentrates in the bulk space in the form of a highly aggregated liquid phase, with strong intermolecular interactions and restricted diffusion. As the pressure continues to increase, its spatial distribution gradually transitions from an aggregated state to a diffused state, with increased intermolecular distances and significant volume expansion. When the pressure reaches 13 MPa, the CO_2-shale oil miscibility can be achieved with no obvious phase boundary at the molecular level. The above visualization results intuitively capture the dynamic process of phase transition, providing clear evidence for the calculation results of the MMP mentioned earlier and further verifying the reliability of the theoretical calculations.

The intermolecular interaction energy can account for this pressure-dependent decreasing trend in IFT. The interaction between CO_2 and shale oil is mainly non-bonding interaction energy, with van der Waals force dominating. Fig. 6 shows the interaction energy between CO_2 and shale oil in bulk phase over time. Under different pressure conditions of 5, 7, 9, 11 and 13 MPa, the stable interaction energies are -185.699, -274.758, -393.254, -522.185 and -680.971 kcal/mol, respectively. As pressure increases, the van der Waals forces strengthen significantly, facilitating a greater penetration of CO_2 molecules into shale oil. This in turn increases the absolute value of intermolecular interaction energies, thereby enhancing the miscibility of the two phases. In general, a larger absolute value of the interaction energy indicates that a miscible state for CO_2 and shale oil can be more easily

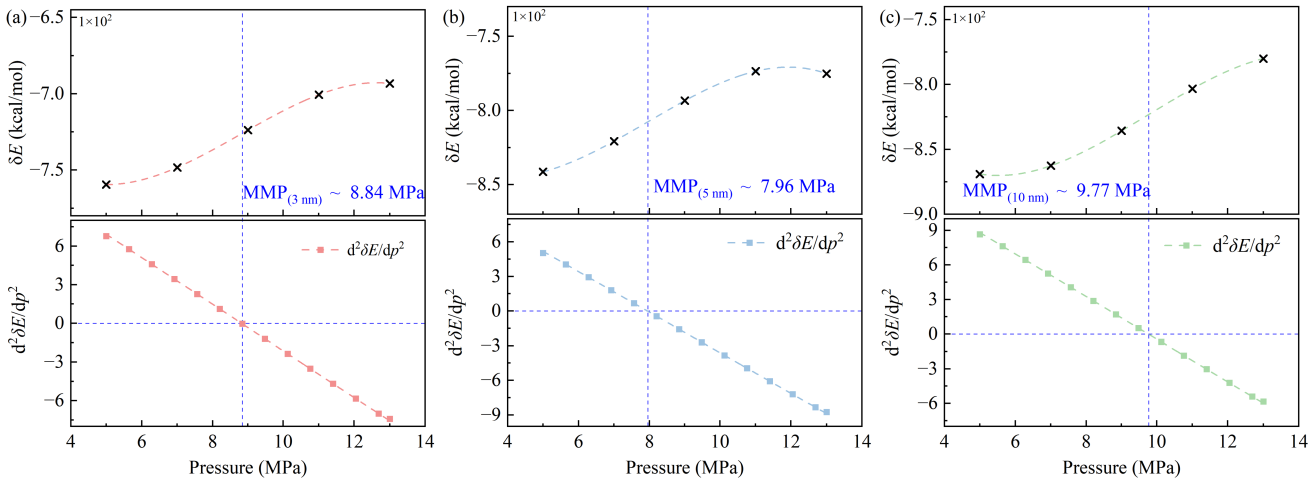

Fig. 7. δE and $\mathrm{d}^2\ \delta E/\mathrm{d}p^2$ versus pressure at 343 K. (a) 3 nm, (b) 5 nm and (c) 10 nm.

achieved.

3.2 Miscible behavior in nanoslits

In this section, molecular simulation is used to investigate the mixing behavior of CO_2 and shale oil under various pressure and temperature conditions, with three pore sizes of 3, 5 and 10 nm.

3.2.1 Determination of MMP by δE

The dynamic evolution of δE can accurately reflect the confinement effect of nanoslits, thereby mapping the thermodynamic phase transition process of fluids from immiscible to miscible state. The calculated interaction energy difference δE between the bulk and confined phases exhibits a rapid rise and subsequent plateau, as shown in Fig. 7.

In the initial stage, the absolute value of δE decreases significantly with increasing pressure, which is caused by the non-equilibrium evolution of the energy difference between wall adsorption and confined-bulk phase interaction. During this stage, the adsorption between shale oil and pore wall is extremely strong. With increasing pressure, the adsorption capacity of the wall decreases rapidly and the negative contribution gradually weakens. Meanwhile, due to the significant density difference between the confined and bulk phase, the absolute value of the confined-bulk phase energy difference declines rapidly, and the positive contribution is also weakened. The contributions of these two effects lead to a sharp change in the absolute value of δE, which fully reflects the dynamic change process of energy dominated by the restriction effect.

As the pressure gradually approaches the MMP, the growth rate of δE slows down significantly. The molecule adsorption on the pore wall gradually tends to saturate with increasing pressure, and the adsorption effect on δE is gradually weakened. At the same time, the density difference between the confined and bulk phase is shrinking. Therefore, the confined-bulk phase energy difference of the fluid gets close to zero, and its contribution to δE is also greatly reduced. When the pressure reaches MMP, the contributions of wall adsorption and confined-bulk phase energy differences to δE cancel each other out, causing the second derivative curve of δE relative to pressure to become zero, as shown in Fig. 7. This critical moment marks the energy equilibrium of confined perturbation and molecular diffusion. At this time, the thermal motion of molecules is sufficient to overcome the adsorption barrier of the pore wall, prompting the qualitative change of fluid from a confined immiscible state to a bulk miscible state. The MMP of CO_2 and shale oil calculated in this study was compared with experimental data (Wang et al., 2024), Monte Carlo simulation results (Xing et al., 2021), and MD simulation results (Sun et al., 2023), as shown in Table 5. Despite differences in temperature and fluid composition, the values in calculated this study were highly consistent with the literature data within the corresponding pressure ranges. Such a high degree of agreement strongly validates the calculation accuracy of the proposed method and fully demonstrates its feasibility and scientific rigor. Taking a 5 nm slit at 343 K shown in Fig. 7(b) as an example, the calculated MMP was 7.96, 3.98 MPa lower than the 11.94 MPa under the bulk condition (Liu et al., 2025). This phenomenon confirms that the confinement effect of nanopores can significantly reduce the CO_2-shale oil MMP. The adsorption between fluid and pore wall weakens the energy barrier of fluid miscibility, such that the molecules can break through the distribution barrier and achieve uniform mixing at lower pressures.

3.2.2 Contribution of pressure to miscibility

In order to deeply explore the pressure effect on mixing behavior, in this section, the relative concentration distributions perpendicular to the wall of fluids were analyzed under different pressures. Obvious adsorption peaks were observed in the concentration distributions of CO_2 and shale oil. As shown in Fig. 8, the amount of shale oil adsorbed near the wall gradually reduces with decreasing pressure, and the amount of free shale oil in the middle of the pore increases significantly. On the contrary, the amount of CO_2 adsorbed near the wall increases. Pressure changes directly affect the interaction strength between molecules and the pore wall as well as between molecules. Under high pressure, the adsorption force between shale oil and the wall is weakened, making shale oil

Table 5. Comparison of the CO_2-shale oil MMP in nanopores determined in this work and literature data.

Reference	Method	Fluid	T (K)	Pore size (nm)	MMP (MPa)
Xing et al. (2021)	Monte Carlo simulation	CO_2 and C_7	353	10	10.40
Sun et al. (2023)	Huff-n-puff process	CO_2 and C_8	333	5	7.93
			353	5	8.20
			373	3	10.28
			373	5	9.93
			373	11	11.00
Wang et al. (2024)	Experimental	CO_2 and mix oil	323	10	7.95
			353	10	10.44
This work	MD	CO_2 and C_{10}	343	3	8.84
			343	5	7.96
			343	10	9.77

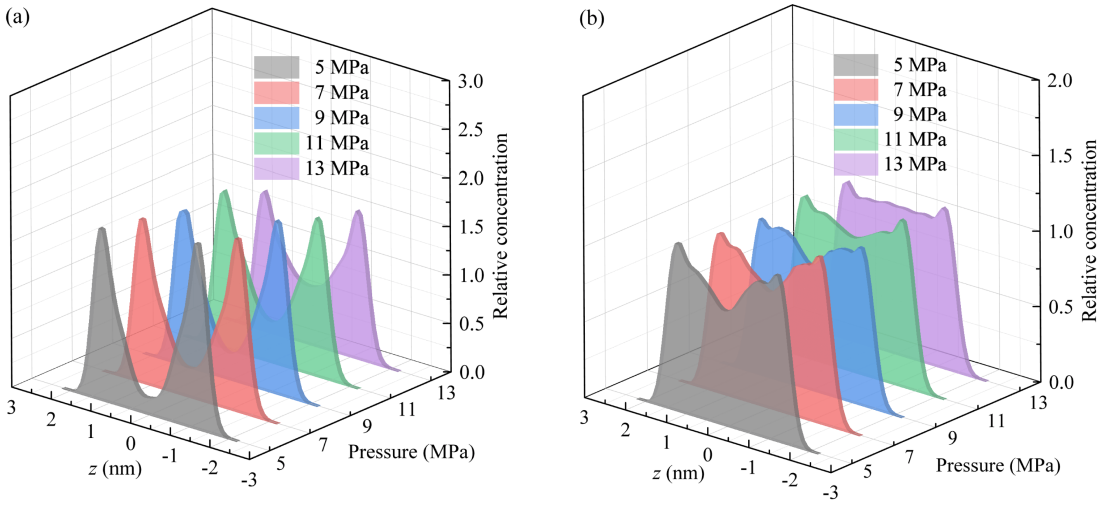

Fig. 8. Relative concentration distribution along the direction perpendicular to the wall in the 3 nm slit at 343 K: (a) Shale oil and (b) CO_2.

more likely to migrate into the pore, while CO_2 is more likely to accumulate on the wall and concentrate in areas conducive to miscibility. This phenomenon is confirmed in the simulation snapshot presented in Fig. 9(a). The adsorption of molecules on the pore wall causes CO_2 and shale oil to be arranged in order, reducing the free energy of the system and creating favorable conditions for the mixing of the two phases. Driven by stronger interactions, CO_2 and shale oil gradually breaks the regional boundaries and reaches a miscible state, as shown in Fig. 9(b).

The influence of pressure on miscibility is also reflected in the molecular diffusion behavior. As shown in Fig. 10, with increasing pressure, the diffusion rate of CO_2 decreases significantly, dropping from 0.42×10^{-7} m^2/s at 5 MPa to 0.2×10^{-7} m^2/s at 13 MPa. The elevated pressure causes CO_2 to aggregate more densely in the pores. Then, the free migration space is compressed and the local molecular collision frequency enhances, which provides direct impetus for breaking the phase interface barrier. In contrast, the diffusion rate of shale oil shows an increasing trend with pressure: Under high pressure, the degree of miscibility between CO_2 and shale oil is strengthened, and the enhanced intermolecular interactions instead weaken the diffusion resistance of shale oil. Such differential diffusion behavior promotes the miscibility of CO_2-shale oil.

3.2.3 Contribution of pore size to miscibility

In order to further investigate the effect of pore size on the MMP, the interaction energies in the 5 and 10 nm slit pore were compared. The MMPs in 3 and 10 nm slits at 343 K were calculated using the method mentioned in Section 2.4, and the results were 8.84 MPa Fig. 7(a), and 9.77 MPa Fig. 7(b), respectively. The effect of pore size on the mixing of CO_2 and shale oil was nonlinear: An upward trend of MMP was witnessed when the pore size was smaller than 5 nm (Fig. S2 in Supplementary file).

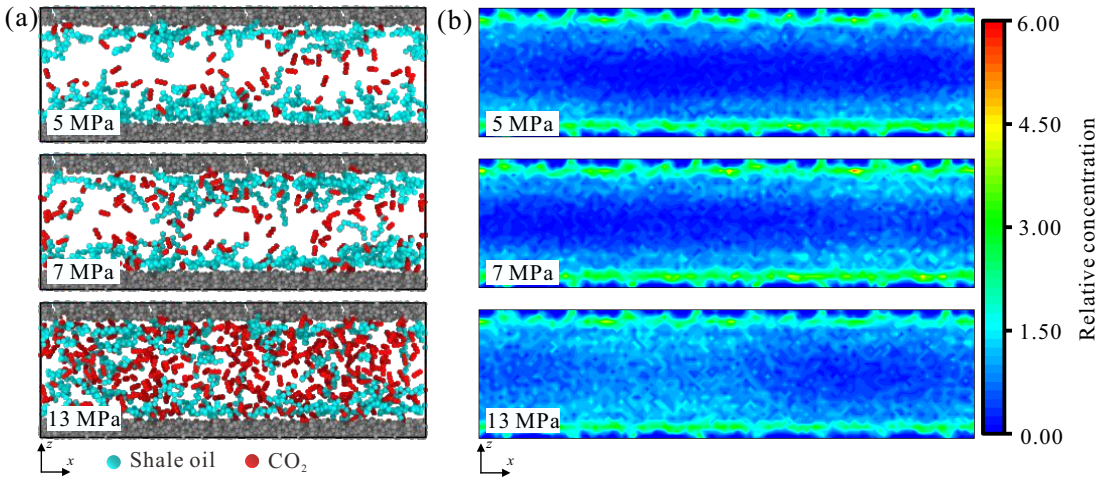

Fig. 9. (a) Simulation snapshots of CO_2 and shale oil and (b) cloud diagram of concentration distribution of shale oil in the 3 nm slit at 343 K.

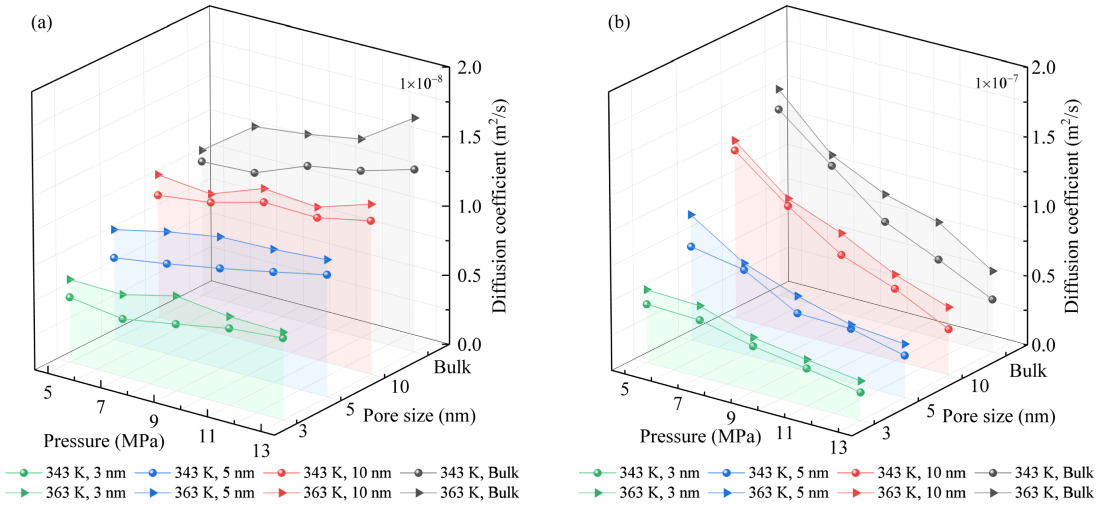

Fig. 10. Diffusion coefficient in slits of different pore sizes at 343 K: (a) Shale oil and (b) CO_2.

The concentration distributions in different pores are displayed in Fig. 11. As the pore size decreases, the adsorption of shale oil on the pore wall increases, and the height of the adsorption peak near the wall increases from 1.1 to 1.7, indicating that the adsorption capacity of the pore wall for shale oil is significantly improved. The adsorption of CO_2 on the wall changes from a single layer to multilayer, which greatly increases the contact possibility between CO_2 and shale oil near the wall. This high contact possibility enhances the interaction energy and allows the mixing of CO_2 and shale oil at a lower pressure. However, when the pore size is reduced to 3 nm, the second adsorption layer of CO_2 on the wall reaches the same height as the first layer. CO_2 occupies more adsorption spots, resulting in a large amount of shale oil peeling off from the wall. In a larger pore, the relative distance between CO_2 and shale oil increases, and more pressure is required to overcome the intermolecular potential energy and achieve a mixed state.

Furthermore, Fig. 10 shows the change in CO_2 and shale oil diffusion coefficients with the pore size. At 343 K and 9 MPa, the diffusion coefficient of CO_2 decreases from 0.66×10^{-7} m^2/s at 10 nm to 0.33×10^{-7} m^2/s at 3 nm as the pore size decreases. This indicates that larger pore size is conducive to the diffusion of molecules, provides wider channels, and promotes the mutual mass transfer of CO_2 and shale oil. However, when the pore size is reduced to a certain extent, especially in pores of 3 nm, the diffusion capacity of CO_2 decreases significantly, resulting in significant restriction of the mixing process.

3.2.4 Contribution of temperature to miscibility

Temperature is also considered to be an important factor for miscibility (Mutailipu et al., 2019). In this work, the kinetic energy of molecules increased and the movement became more violent at higher temperatures, weakening the adsorption between molecules and pore walls. Meanwhile, the increase in temperature also affected the collision frequency and energy between CO_2 and other substance molecules, which was unfavorable for the formation of miscibility.

On the basis of the method proposed in this paper, the interaction energy differences between the bulk phase and pore conditions at 363 K were calculated (Fig. S1 in Supplementary

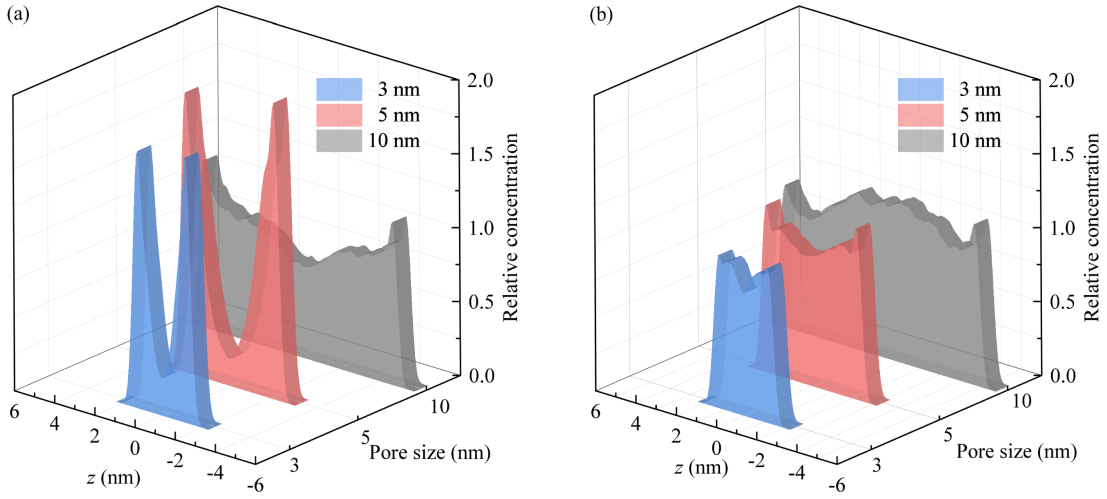

Fig. 11. Relative concentration distribution along the direction perpendicular to the wall in the 9 MPa at 343 K: (a) Shale oil and (b) CO_2.

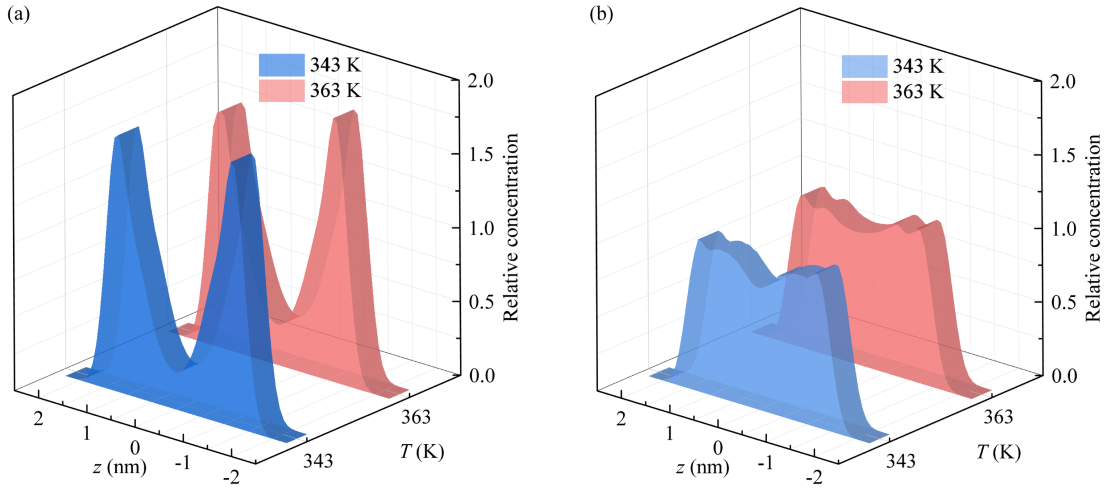

Fig. 12. Relative concentration distribution along the direction perpendicular to the wall in the 3 nm slit at 9 MPa: (a) Shale oil and (b) CO_2.

Table 6. The MMP of the CO_2 and shale oil in this study.

T (K)	Pore size (nm)	MMP (MPa)
343	3	8.84
	5	7.96
	10	9.77
	Bulk	11.94
363	3	9.83
	5	8.81
	10	10.62

file). It was found that the MMP corresponding to each pore condition at this temperature was higher than that under the same conditions at 343 K. For instance, at 3, 5 and 10 nm pores, the MMP values at 363 K were 9.83, 8.81, and 10.62 MPa, respectively (Table 6). The main reason for this phenomenon is that increased temperature enhances the kinetic energy of CO_2 and shale oil molecules, and this increase in kinetic energy enlarges the relative distance between molecules, thereby weakening their mutual interaction forces and making it more difficult for the miscibility of CO_2 and shale oil. Meanwhile, this enhanced kinetic energy also weakens the adsorption between molecules and pore walls, reducing the retention of oil phase on pore walls and resulting in fewer effective intermolecular collisions. These two mechanisms synergistically hinder CO_2-shale oil miscibility, ultimately causing an increase in MMP. This was also confirmed by the fluid concentration distribution. Fig. 12 shows the relative concentration distribution at different temperatures with 9 MPa when the pore size is 3 nm. It can be observed that the adsorption peak at 363 K is significantly lower than that at 343 K. The rise in temperature makes it easier for CO_2 and shale oil to desorb from the wall surface, reducing the stability of the adsorption layer and the concentration on the wall surface (Huang et al., 2025). As a result, the probability of collision between CO_2 and shale oil decreased, leading to an increase in MMP at high temperatures.

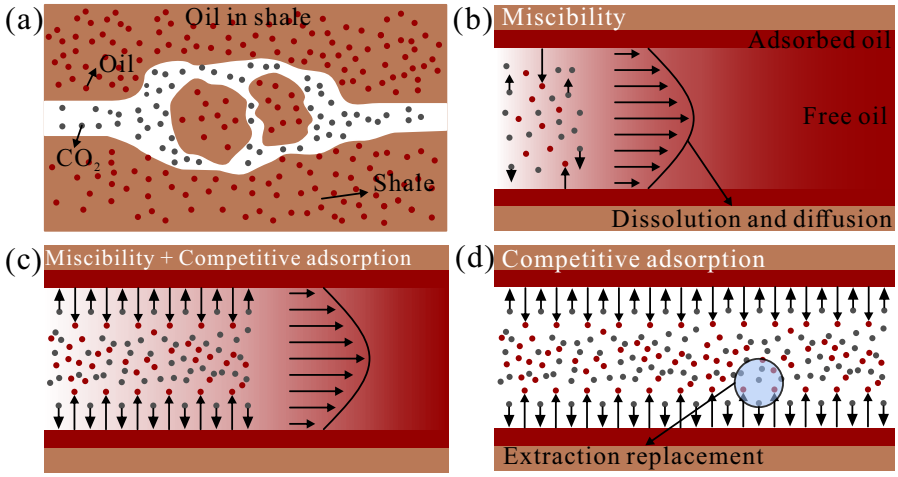

Fig. 13. Schematic of CO_2-ESOR mechanism: (a) Initial stage, (b) early stage, (c) middle stage and (d) later stage.

3.3 Mechanism of CO_2-ESOR

During CO_2-ESOR, the miscibility process, as the most significant mechanism, is essentially the synergistic evolution of thermodynamic and kinetic properties between CO_2 and the shale oil system in nanopores. When CO_2 is injected into shale reservoirs, it dissolves into the oil phase through interfacial mass transfer within nanoslits, as shown in Figs. 13(a) and 13(b). Thus, oil viscosity is reduced and the oil volumetric expansion is induced, thereby changing trapped oil into a mobile state. When the system pressure exceeds the MMP, the miscibility between CO_2 and shale oil significantly increases, the fluid properties are markedly improved and the recovery efficiency is substantially enhanced. The confinement effect of pore size significantly reduces the MMP, making CO_2 and shale oil more miscible. However, when the pore size decreases below a certain threshold, the contributory confinement effect on CO_2-shale oil miscibility is weakened. Similarly, as temperature rises, the MMP in the system increases to some extent and higher gas injection pressure is required to achieve the same recovery efficiency. Furthermore, competitive adsorption between CO_2 and shale oil exists within nanopores, as shown in Figs. 13(c) and 13(d), while the coupling mechanism of adsorption energy still requires further in-depth investigation.

4. Conclusions

In this work, the miscibility behavior between CO_2 and shale oil under the reservoir conditions were studied through theoretical methods and MD simulations. The main conclusions are as follows:

1) The confinement effect was quantified by the evolution of the energy difference between bulk and confined phase with pressure, and a method of MMP estimation in the CO_2 and shale oil system was established. The calculation results were consistent with the results using other methods in the literature.
2) As the pressure reaches MMP, the energy equilibrium of confined perturbation and molecular diffusion is achieved. When the thermal motion of the molecules is sufficient to overcome the adsorption barrier of the pore wall, the fluid can change from a confined immiscible state to a bulk miscible state.
3) The confinement effect can reduce the MMP of CO_2 and shale oil. However, when the pore size decreases to a certain extent, the significant decrease in the fluid diffusion coefficient and the increase in the thickness of the pore wall adsorption layer lead to reduced mass transfer efficiency, thereby causing a remarkable increase in MMP.
4) The temperature increase enhances the molecular thermal motion and weakens the adsorption between molecules and pore walls, resulting in a decreased collision probability between CO_2 and shale oil and a reduction in effective intermolecular interactions, which is detrimental to fluid miscibility.

Acknowledgements

The authors acknowledge the financial support from the National Natural Science Foundation (Nos. 52304059 and 52204039), and the Natural Science Foundation of Shandong Province (Nos. ZR2022QE038 and ZR2022QB046).

Supplementary file

https://doi.org/10.46690/ager.2025.08.03

Conflict of interest

The authors declare no competing interest.

References

Abdurrahman, M., Permadi, A. K., Arsad, A., et al. Minimum CO_2 miscibility pressure evaluation using interfacial tension (IFT) and slim-tube hybrid tests. ACS Omega, 2023, 8(9): 8703-8711.

Alafnan, S. Carbon dioxide and methane sequestration in

organic-rich shales: Nanoscale insights into adsorption and transport mechanisms. Journal of Energy Resources Technology-Transactions of the Asme, 2022, 144(7): 073010.

Allen, M. P., Tildesley, D. J. Computer Simulation of Liquids. Oxford, UK, Oxford University Press, 2017.

Bu, H., Ju, Y., Tan, J., et al. Fractal characteristics of pores in non-marine shales from the Huainan coalfield, eastern China. Journal of Natural Gas Science and Engineering, 2015, 24: 166-177.

Bu, Y., Sun, Q., Fu, S., et al. Nanometer-scale CO_2-shale oil minimum miscibility pressure calculations based on modified PR-EOS. Geofluids, 2023, 2023(1): 4282387.

Collell, J., Ungerer, P., Galliero, G., et al. Molecular simulation of bulk organic matter in type II shales in the middle of the oil formation window. Energy & Fuels, 2014, 28(12): 7457-7466.

Dinpajooh, M., Bai, P., Allan, D. A., et al. Accurate and precise determination of critical properties from Gibbs ensemble Monte Carlo simulations. Journal of Chemical Physics, 2015, 143(11): 114113.

Dong, C., Hoffman, B. T. Modeling gas injection into shale oil reservoirs in the sanish field, North Dakota. Paper URTeC 1581998 Presented at SPE/AAPG/SEG Unconventional Resources Technology Conference, Denver, Colorado, 12-14 August, 2013.

Dong, P., Liao, X., Chen, Z., et al. An improved method for predicting CO_2 minimum miscibility pressure based on artificial neural network. Advances in Geo-Energy Research, 2019, 3(4): 355-364.

Dong, X., Xu, W., Liu, H., et al. Molecular insight into the oil displacement mechanism of CO_2 flooding in the nanopores of shale oil reservoir. Petroleum Science, 2023, 20(6): 3516-3529.

Edwards, R. W. J., Celia, M. A., Bandilla, K. W., et al. A model to estimate carbon dioxide injectivity and storage capacity for geological sequestration in shale gas wells. Environmental Science & Technology, 2015, 49(15): 9222-9229.

Fang, T., Zhang, Y., Liu, J., et al. Molecular insight into the miscible mechanism of CO_2/C_{10} in bulk phase and nanoslits. International Journal of Heat and Mass Transfer, 2019, 141: 643-650.

Firouzi, M., Rupp, E. C., Liu, C., et al. Molecular simulation and experimental characterization of the nanoporous structures of coal and gas shale. International Journal of Coal Geology, 2014, 121: 123-128.

Hassan, A., Elkatatny, S., Abdulraheem, A. Intelligent prediction of minimum miscibility pressure (MMP) during CO_2 flooding using artificial intelligence techniques. Sustainability, 2019, 11(24): 7020.

Hawthorne, S. B., Miller, D. J., Grabanski, C. B., et al. Experimental determinations of minimum miscibility pressures using hydrocarbon gases and CO_2 for crude oils from the bakken and cut bank oil reservoirs. Energy & Fuels, 2020, 34(5): 6148-6157.

Hawthorne, S. B., Miller, D. J., Jin, L., et al. Rapid and simple capillary-rise/vanishing interfacial tension method to determine crude oil minimum miscibility pressure: Pure and mixed CO_2, methane, and ethane. Energy & Fuels, 2016, 30(8): 6365-6372.

Hou, B., Chang, Z., Fu, W., et al. Fracture initiation and propagation in a deep shale gas reservoir subject to an alternating-fluid-injection hydraulic-fracturing treatment. SPE Journal, 2019, 24(4): 1839-1855.

Huang, Y., Mao, X., Yang, D., et al. Probing the interactions between asphaltenes and a PEO-PPO demulsifier at oil-water interface: Effect of temperature. Journal of Colloid and Interface Science, 2025, 678: 1096-1111.

Huang, F., Xu, R., Jiang, P., et al. Pore-scale investigation of CO_2/oil exsolution in CO_2 huff-n-puff for enhanced oil recovery. Physics of Fluids, 2020, 32(9): 092011.

Hui, G., Chen, Z., Schultz, R., et al. Intricate unconventional fracture networks provide fluid diffusion pathways to reactivate pre-existing faults in unconventional reservoirs. Energy, 2023, 282: 128803.

Lashgari, H. R., Sun, A., Zhang, T., et al. Evaluation of carbon dioxide storage and miscible gas EOR in shale oil reservoirs. Fuel, 2019, 241: 1223-1235.

Li, J., Chen, Z., Wu, K., et al. A multi-site model to determine supercritical methane adsorption in energetically heterogeneous shales. Chemical Engineering Journal, 2018, 349: 438-455.

Li, J., Li, X., Wang, X., et al. Water distribution characteristic and effect on methane adsorption capacity in shale clay. International Journal of Coal Geology, 2016, 159: 135-154.

Li, S., Ye, Z., Wang, J., et al. Effects of fracturing fluid composition and other factors on improving the oil imbibition recovery of shale reservoir. Capillarity, 2023, 9(3): 45-54.

Liu, B., Lei, X., Feng, D., et al. Nanoconfinement effect on the miscible behaviors of CO_2/shale oil/surfactant systems in nanopores: Implications for CO_2 sequestration and enhanced oil recovery. Separation and Purification Technology, 2025, 356: 129826.

Liu, B., Shi, J., Sun, B. J., et al. Molecular dynamics simulation on volume swelling of CO_2-alkane system. Fuel, 2015, 143: 194-201.

Liu, J., Yang, Y., Sun, S., et al. Flow behaviors of shale oil in kerogen slit by molecular dynamics simulation. Chemical Engineering Journal, 2022, 434: 134682.

Lv, W., Dong, M. Z., Sarma, H., et al. Effects of CO_2-philic nonionic polyether surfactants on miscibility behaviors of CO_2-hydrocarbon systems: Experimental and simulation approach. Chemical Engineering Journal, 2023, 464: 142701.

Mohammadian, E., Mohamadi-Baghmolaei, M., Azin, R., et al. RNN-based CO_2 minimum miscibility pressure (MMP) estimation for EOR and CCUS applications. Fuel, 2024, 360: 130598.

Mutailipu, M., Jiang, L., Liu, X., et al. CO_2 and alkane minimum miscible pressure estimation by the extrapolation of interfacial tension. Fluid Phase Equilibria, 2019, 494: 103-114.

Peng, F., Wang, R., Guo, Z., et al. Molecular dynamics simulation to estimate minimum miscibility pressure for

oil with pure and impure CO_2. Journal of Physics Communications, 2018, 2(11): 115028.

Pi, Z., Peng, H., Jia, Z., et al. Coupling mechanisms of displacement and imbibition in pore-fracture system of tight oil reservoir. Capillarity, 2023, 7(1): 13-24.

Plimpton, S. Fast parallel algorithms for short-range molecular dynamics. Journal of Computational Physics, 1995, 117(1): 1-19.

Prasetyo, L., Do, D. D., Nicholson, D. A coherent definition of henry constant and isosteric heat at zero loading for adsorption in solids - an absolute accessible volume. Chemical Engineering Journal, 2018, 334: 143-152.

Raza, A., Mahmoud, M., Alafnan, S., et al. H2, CO_2, and CH_4 adsorption potential of kerogen as a function of pressure, temperature, and maturity. International Journal of Molecular Sciences, 2022, 23(21): 12767.

Rogala, A., Ksiezniak, K., Krzysiek, J., et al. Carbon dioxide sequestration during shale gas recovery. Physicochemical Problems of Mineral Processing, 2014, 50(2): 681-692.

Safaei, A., Kazemzadeh, Y., Riazi, M. Mini review of miscible condition evaluation and experimental methods of gas miscible injection in conventional and fractured reservoirs. Energy & Fuels, 2021, 35(9): 7340-7363.

Shaver, R. D., Robinson, R. L., Gasem, K. A. M. An automated apparatus for equilibrium phase compositions, densities, and interfacial tensions: Data for carbon dioxide plus decane. Fluid Phase Equilibria, 2001, 179(1-2): 43-66.

Stankiewicz, A., Ionkina, N., Motherwell, B., et al. Kerogen density revisited-lessons from the duvernay shale. Paper URTEC 2157904 Presented at Proceedings of the 3rd Unconventional Resources Technology Conference, San Antonio, Texas, 20-22 July, 2015.

Sun, H., Li, H. A new three-phase flash algorithm considering capillary pressure in a confined space. Chemical Engineering Science, 2019, 193: 346-363.

Sun, Q., Bhusal, A., Zhang, N., et al. Molecular insight into minimum miscibility pressure estimation of shale oil/CO_2 in organic nanopores using CO_2 huff-n-puff. Chemical Engineering Science, 2023, 280: 119024.

Teklu, T. W., Alharthy, N., Kazemi, H., et al. Phase behavior and minimum miscibility pressure in nanopores. SPE Reservoir Evaluation & Engineering, 2014, 17(3): 396-403.

Ungerer, P., Collell, J., Yiannourakou, M. Molecular modeling of the volumetric and thermodynamic properties of kerogen: Influence of organic type and maturity. Energy & Fuels, 2015, 29(1): 91-105.

Wan, Y., Jia, C., Lv, W., et al. Recovery mechanisms and formation influencing factors of miscible CO_2 huff-n-puff processes in shale oil reservoirs: A systematic review. Advances in Geo-Energy Research, 2024, 11(2): 88-102.

Wang, Z., Liu, T., Liu, S., et al. Adsorption effects on CO_2-oil minimum miscibility pressure in tight reservoirs. Energy, 2024, 288: 129815.

Wang, R., Peng, F., Song, K., et al. Molecular dynamics study of interfacial properties in CO_2 enhanced oil recovery. Fluid Phase Equilibria, 2018, 467: 25-32.

Wu, K., Li, X., Guo, C., et al. A unified model for gas transfer in nanopores of shale-gas reservoirs: Coupling pore diffusion and surface diffusion. SPE Journal, 2016, 21(5): 1583-1611.

Wu, Z., Sun, Z., Shu, K., et al. Mechanism of shale oil displacement by CO_2 in nanopores: A molecular dynamics simulation study. Advances in Geo-Energy Research, 2024, 11(2): 141-151.

Xing, X., Feng, Q., Zhang, W., et al. Vapor-liquid equilibrium and criticality of CO_2 and n-heptane in shale organic pores by the Monte Carlo simulation. Fuel, 2021, 299: 120909.

Yu, X., Li, J., Chen, Z., et al. Molecular dynamics computations of brine-CO_2/CH_4-shale contact angles: Implications for CO_2 sequestration and enhanced gas recovery. Fuel, 2020, 280: 118590.

Yu, X., Li, J., Chen, Z., et al. Determination of CH_4, C_2H_6 and CO_2 adsorption in shale kerogens coupling sorption-induced swelling. Chemical Engineering Journal, 2021, 410: 127690.

Yuan, L., Zhang, Y., Liu, S., et al. Molecular dynamics simulation of CO_2-oil miscible fluid distribution and flow within nanopores. Journal of Molecular Liquids, 2023, 380: 121769.

Zhan, S., Su, Y., Jin, Z., et al. Effect of water film on oil flow in quartz nanopores from molecular perspectives. Fuel, 2020, 262: 116560.

Zhang, K., Jia, N., Li, S., et al. Nanoscale-extended correlation to calculate gas solvent minimum miscibility pressures in tight oil reservoirs. Journal of Petroleum Science and Engineering, 2018a, 171: 1455-1465.

Zhang, K., Jia, N., Li, S., et al. Thermodynamic phase behaviour and miscibility of confined fluids in nanopores. Chemical Engineering Journal, 2018b, 351: 1115-1128.

Zhang, K., Jia, N., Zeng, F., et al. A new diminishing interface method for determining the minimum miscibility pressures of light oil-CO_2 systems in bulk phase and nanopores. Energy & Fuels, 2017, 31(11): 12021-12034.

Zhang, L., Wu, K., Chen, Z., et al. Molecular-scale friction at a water-graphene interface and its relationship with slip behavior. Physics of Fluids, 2020a, 32(9): 092001.

Zhang, M., Zhan, S., Jin, Z. Recovery mechanisms of hydrocarbon mixtures in organic and inorganic nanopores during pressure drawdown and CO_2 injection from molecular perspectives. Chemical Engineering Journal, 2020b, 382: 122808.